THE SURFACE INTERPOLATION METHOD FOR DAMAGE LOCALIZATION IN PLATES

M.P. Limongelli[1]

[1] *Department ABC, Architecture, Built Environment and Construction Engineering*

Politecnico di Milano

Piazza Leonardo da Vinci 32, 20133 Milano

e-mail: mariapina.limongelli@polimi.it

phone: +39 02 23994228

fax : +39 02 23994220

Abstract: This paper presents a vibration based procedure for locating reductions of stiffness in plate-like structures. This procedure is a generalization to the two-dimensional case of the Interpolation Method (IM) previously published by the author. The method is based on the definition of a damage sensitive feature in terms of the accuracy of a spline function in interpolating the operational displacement shapes of the structure. In the previous works the IM was applied as a method of level 2 for damage identification that is able to detect and localize damage. In this paper an analytical relationship between the damage feature and the curvature discontinuity is proved. For two-dimensional structures, a bi-cubic spline surface is defined herein to interpolate the operational shapes. In order to account for the uncertainties related to random variations of the damage feature, an approach based on the definition of an acceptable value of the probability of false alarm was formerly proposed by the author. A simplified version of the algorithm is presented herein for the case ~~that~~ whereby the statistical distribution of the damage feature in the original (undamaged) state is not available, and the damage diagnosis has to be carried out ~~basing~~ based on just two sets of responses recorded on the original and on the (possibly) damaged structure. The proposed two-dimensional Surface Interpolation Method (SIM) is checked herein ~~through~~ via numerical simulations using the FE model of a plate and modeling local reductions of stiffness through a reduction of the elastic modulus of the material. ~~Validation r~~Results demonstrate that the algorithm provides a reliable tool for damage identification of plate-like structures. The performance of the method can be affected by noise in recorded data, ~~but~~ however a careful choice of the accepted probability of false alarm can reduce this drawback.

Keywords: Damage localization, Frequency Response Functions, Interpolation Method, Gibbs phenomenon for splines.

1. INTRODUCTION

Plates are important structural elements, widely used in several engineering applications and the monitoring of their condition is an important aspect for the assessment of the global structural condition. Non-destructive damage detection techniques traditionally consist ofin visual inspections and/or non-destructive testing (acoustic, ultrasonic, magnetic field, thermal field methods) that may effectively detect damage but only if its location is already known and limited to a portion of the structure.

A different approach, that which overcomes these difficulties, consists of usingin vibration based damage identification methods based on the idea that damage in a structure causes a change inof its dynamic response characteristics that is reflected by a change of thein the vibration response to vibrations. The application of such methods requires the acquisition of structural responses over time and the extraction from these responses of damage-sensitive properties (features) from these responses allowing the detecting detection of the difference between the undamaged and the damaged structure.

In the last twenty years several vibration-based damage localization methods, based on different features, have been proposed in literature. A number of these use modal parameters as damage sensitive features such as:: modal shapes or their derivatives (modal rotation [1], modal curvature [2]-[4]), modal strain energy [5] and, modal flexibility [6], among others. In reference [7] a comprehensive state of the art of modal methods is reported.

One drawback of modal methods is relatedrelates to the need of to estimating estimate modal parameters, i.e.: the results are dependent on the quality of modal parameters. This, especially in the case of mild damage, introduces errors related to experimental noise that sometime hampers athe correct identification of damage. The influence of noise is particularly important if modal shapes are used for localization of damage. This makes more feasible, for damage localization, approaches based on the use of operational deformed shapes calculated from frequency response functions such as the Gapped Smoothing Method, the Frequency Response Curvature Method and the Interpolation method respectively proposed in references [8], [9] and [10] for beam--like structures. More recently the Frequency Shift Curve Method has been proposed in reference [11] based on the derivative of the equivalence between the 'frequency shift curve' due to an auxiliary mass and the mode shape square.

A large part of both modal and non-modal damage identification methods has been initially proposed and applied for beam-like structures and later extended to bi-dimensional structures. In reference [12] and [13] respectively the strain energy method and the gapped smoothing method are extended to plates. ~~and m~~More recently the Frequency Shift Surface, based on the Frequency Shift Curve Method was extended to plates-like structures [14]. Wu and Law ~~in reference~~ [15] proposed ~~for damage localization in plates~~ the uniform load surface defined as the vertical displacement of a~~the~~ plate under uniform load for damage localization in plate-like structures.

The author of this paper recently proposed the Interpolation Method (IM) for damage localization in beam-like structures. In references [17], [18] and [19] the IM was applied respectively to the case of a real instrumented bridge, to a multistory frame and to a real instrumented building~~s~~ subjected to seismic excitation. The focus of this paper is on the extension of the IM to bi-dimensional structure such as plates.

This method uses accelerations recorded in a number of locations on the structure to detect local variations of stiffness with respect to a reference configuration. Such variations are pointed out by local changes of the operational deflection shapes (ODS) recovered from experimental frequency response functions (FRFs). An ODS is the deformed shape of a structure subjected to a harmonic excitation. If the frequency of the excitation is close to a modal frequency of the structure, the ODS is dominated by the relevant mode shape, otherwise the ODS derives from the superposition of several mode shapes. A localized reduction of stiffness induces a local reduction of smoothness of the ODS~~s~~ at the damaged section. In a previous paper, it was shown by the author that an effective technique to identify local reductions of smoothness in beam-like structures is based on the interpolation of their response to vibrations through a cubic spline function [18].

In reference [10] it was shown that the capability of the IM to localize damage is due to the so-called 'Gibbs phenomenon for splines'. This phenomenon numerically enhances local reductions of smoothness thus causing a sharp increase of the interpolation error at locations of curvature discontinuity. In reference [20] the modal SIM, two-dimensional extension of the previously published modal IM, was proposed and applied to the example of a plate already used by other researchers (see ~~reference~~ [14]). In all the previous applications of the IM and of the SIM the method was used as a level 2 damage identification algorithm meaning a method able to detect and locate damage. In those studies the Gibbs phenomenon was explained through examples from a numerical point of view and no attempt was done to relate the curvature discontinuity to the jump of the interpolating function. In the present work, ~~we provide~~ an extensive description of the theoretical background of the method together with a rigorous proof of the analytical relationship

between the damage feature and the amplitude of damage is provided. The proof of this is one of the main ~~novelties~~ novel contributions of this paper. The investigation of the effect of noise on the accuracy of damage localization is another novel aspect that was not acknowledged in ~~the~~ previous studies and ~~that~~ so is considered herein.

The outline of the paper is as follows. In section 2, a detailed description of bi-cubic spline interpolation is reported, together with a description of the Gibbs phenomenon for splines which is presented and discussed with reference to a simple case. In section 3 the extension of the Surface Interpolation Method is outlined and in sections 4 to 6 the result of its applications to both numerical and experimental examples are reported. In the appendix of the paper the proof of the Gibbs phenomenon is given and the computation of the maximum overshoot between a function with a discontinuity and its interpolation is reported.

2. SPLINE INTERPOLATION

The Surface Interpolation Method proposed herein for damage localization in plates, is based on the interpolation of the operational displacement shapes of the plate via a bi-cubic spline function.

In this section ~~are recalled~~ some properties of this family of functions that make them useful for damage localization are described. Furthermore, in order to make the paper self-contained, the mathematical details of cubic and bi-cubic spline interpolations are also reported.

2.1. Properties of spline interpolation

The process of interpolation consists in recovering continuous data from a discrete set of data, ~~basing~~ based ~~of~~ on a given model; this is a fundamental operation in several fields where resampling of a limited set of data is needed. One of these fields is image processing where there is often the need to reconstruct the data lost in a previous image sampling process in order to change the size of images ~~-~~and/or to correct spatial distortions.

The use of cubic spline functions in image resampling is widespread for two main reasons that make the cubic spline functions a good compromise between computational burden and interpolation accuracy [21].

a) they are the smoothest among all the functions of class C^2 that interpolate a given set of data: a cubic spline minimizes the least square errors of the function values and of its derivatives at the interpolation points [22]
b) they are piecewise low order polynomial functions thus they are stable (small variations of the data at one interpolation point does not produce sensible variations of the interpolating function as occurs on the contrary for higher order polynomial functions) and with a local

character (a steep variation of the data in a small interval, affectings only locally the interpolating function)

On the other side, the high smoothness of the spline function may be a drawback for a reliable interpolation in case of non--smooth regions of curves or surfaces. This is due to a phenomenon known as '*Gibbs' phenomenon of splines*' occurring when the spline interpolates functions with discontinuities: the spline interpolation oscillates near a discontinuous point and has an overshoot (values higher than those of the function to be interpolated [23]). In other words, in a region close to a discontinuity the requirement to have ofa smooth curve leads the interpolating cubic spline to oscillate between data constraints hence to an increase of the interpolation error occurs.

This phenomenon is the main reason why in some applications the condition about the continuity of the second derivative is relaxed and only conditions about the continuity of the function and of its first derivative are imposed [24].

Herein this 'drawback' related to the Gibbs' phenomenon is turned into a 'useful feature' and used as a sort of 'curvature discontinuity detector'. At locations where a discontinuity of the second derivative (proportional to the curvature) occurs, the Gibbs phenomenon causes an overshoot (high value of the interpolation error). The amplitude of the overshoot is proportional to the discontinuity. A proof and the expression of the overshoot between the second derivative of the function and of its spline interpolation is reported in the appendix of the paper. If the interpolation is repeated in two configurations corresponding to different amplitudes of the discontinuity – there is a variation of overshoot that is of the interpolation error. Namely if the discontinuity of curvature (damage) increases at a given location, the interpolation error at that location increases proportionally. This is the reason why the variation of the interpolation error is assumed herein as the damage feature.

The advantage of the Interpolation Method with respect to other methods based on the use of variations of curvature as damage detecting features is that the IM localizes variations of curvature without actually computing curvature. The discontinuities of curvature are localized as locations where the interpolation of the operational shape exhibits the Gibbs phenomenon. -This allows to overcome all the drawbacks related to the computation of curvature for noisy (real world) signals.

Regarding the choice of the cubic spline as the interpolant, it depends on the circumstance that this function is the one that allows maximizing the value of the overshoot due to the Gibbs phenomenon thus enhancing the effectiveness of the damage localization method.

From this point of view the use of the cubic spline is more effective with respect to other interpolating functions, for example polynomials, even if with respect to the latter, the computational cost of interpolation might be increasedmay increase.

In the following ~~of this~~sub-~~-~~section, for the sake of clarity and to make the paper self-~~-~~contained, more details about the bi-cubic spline interpolation and about the Gibbs phenomenon for splines are reported.

2.2. Bi-cubic spline interpolation

A bi-cubic spline interpolation can be used to interpolate a function~~n~~ $F(x, y)$ with a smooth surface, ~~that is a function that~~which guarantees continuity ~~of~~ of the first and second derivatives.

A bi-cubic spline can be thought as a surface constructed from families of cubic spline functions.

Given the values of a function $F(x, y)$ defined on a rectangular grid of n_{l+2} x n_{p+2} nodes, consider the following equation:

$$s(x,y):\ s_p(x,y)=\sum_{j=0}^{3} c_{jp}(x)(y-y_p)^j \qquad y\in\left\lfloor y_p, y_{p+1}\right\rfloor \qquad \text{with } p=0,\ 2...,\ n_p \tag{1}$$

For each value of x, equation (1~~1~~) gives a spline function along y (see black curves in Figure 1~~Figure 1~~). When x varies, the coefficients $c_{jp}(x)$ also vary and a family of cubic spline functions $s(x,y)$ is obtained.

If also the coefficients $c_{jp}(x)$ are defined by cubic spline functions (see red line in Figure 1~~Figure 1~~) in each sub-area defined by $x\in[x_l, x_{l+1}];\ y\in\left\lfloor y_p, y_{p+1}\right\rfloor$ they can be written as:

$$c_{jp}(x):\qquad c_{jp,l}(x)=\sum_{i=0}^{3} a_{jp,il}(x-x_l)^i \qquad x\in[x_l, x_{l+1}];\ y\in\left\lfloor y_p, y_{p+1}\right\rfloor; \tag{2}$$

p=0, 2..., n_p, l=0, 2..., n_l

In this case, the following function $S(x,y)$ is a bi-cubic spline function defined through its restrictions to sub-areas as:

$$S(x,y):\qquad S_{l,p}(x,y)=\sum_{j=0}^{3}\sum_{i=0}^{3} a_{jp,il}(x-x_l)^i(y-y_p)^j \qquad x\in[x_l, x_{l+1}];\ y\in\left\lfloor y_p, y_{p+1}\right\rfloor \tag{3}$$

In order to calculate the coefficients $a_{jp,il}$ of the bi-cubic spline function, a two steps process can be applied.

First, on the basis of the known values of the function $F(x,l)$ at the nodes, a sequence of one-dimensional cubic splines, for example along y, is constructed for all the x values on the grid.

For the l-th line of the grid along y ($x=x_l$) the cubic spline function is defined as:

$$s(x_l,y):\qquad s_p(x_l,y)=\sum_{j=0}^{3} c_{jp}(x_l)(y-y_p)^j \qquad y\in\left\lfloor y_p, y_{p+1}\right\rfloor \qquad l=0,\ 1,....,n_l+1 \tag{4}$$

Formattato: Spagnolo (Spagna, ordinamento tradizionale), Controllo ortografia e grammatica

The coefficients $c_{jp}(x_l)$ at the l-th grid line are calculated basing on the interpolation and continuity conditions at nodes $(x_1, y_1), (x_l, y_2).....(x_{n_l}, y_{n_p})$ as described previously for the cubic spline interpolation.

The second step of the procedure is the cubic spline interpolation, for every $y=y_p$, $p=0, 1, 2\ldots, n_p+1$ of the values $c_{jp}(x)$ along x. For the p-th gridline ($y=y_p$) along x:

$$c_{jp}(x): \qquad c_{jp,l}(x) = \sum_{i=0}^{3} a_{jp,il}(x - x_l)^i \qquad x \in [x_l, x_{l-1}];\ y = y_p \tag{5}$$

where the coefficients $a_{jp,il}$ are determined basedingon ~~and on~~ boundary conditions at nodes $x=0$ and $x=x_{nl}$ and on continuity and interpolation conditions imposed on function $c_{jp}(x)$ at the internal nodes $(x_1, y_p), (x_2, y_p).....(x_{n_l}, y_p)$

$$\begin{Bmatrix} c_{l,p}(x_l) = c_{l-1,p}(x_l) \\ c'_{l,p}(x_l) = c'_{l-1,p}(x_l) \\ c''_{l,p}(x_l) = c''_{l-1,p}(x_l) \\ c_{l,p}(x_l) = F_{l,p} \end{Bmatrix} \qquad l=1, 2, n_l \qquad p = 1, 2\ \ldots n_p \tag{6}$$

These conditions give the following system in the unknown coefficients $a_{jp,il}$.(i=0,1,..3)

$$\begin{cases} a_{jp,ol} = a_{jp,o(l-1)} + a_{jp,1(l-1)}k_l + a_{jp,2l}k_l^2 + a_{jp,3(l-1)}k_l^3 \\ a_{1,l} = a_{jp,1(l-1)} + 2a_{jp,2(l-1)}k_p + 3a_{jp,3(l-1)}k_l^2 \\ a_{jp,2(l-1)} = a_{jp2(l-1)} + 3a_{jp,3(l-1)}k_l \\ a_{jp,ol} = c_{jp}(x_l) \end{cases} \tag{7}$$

where $k_l = x_l - x_{l-1}$.

Once the coefficients $a_{jp,ol}$ are known, the values of the bi-cubic interpolation can ~~be~~ finally be calculated using equation (~~3~~3).

Formattato: Spagnolo (Spagna, ordinamento tradizionale), Controllo ortografia e grammatica

2.3. The Gibbs phenomenon for cubic splines and the variation of the interpolation error

A complete analytic discussion of the Gibbs phenomenon for splines and of its mathematical properties is reported in several papers [23]-[25]. In the Appendix of this~~e~~ paper the proof that the maximum overshoot due to the Gibbs phenomenon is proportional to the magnitude of the discontinuity is reported. This section contains a qualitative description of this phenomenon, aimed to explain the choice of the cubic splines as interpolating functions for damage detection purposes. In Figure 2~~Figure 2~~ two piecewise functions composed by line segments and arcs of a circle are reported. In these functions,~~ that~~ which can be considered as two deformed configurations, there are some nodes where a jump ~~of~~ in the curvature occurs, as reported in the figure.

In configuration 1 there are discontinuities of curvature at locations:

at x=1 from 0 to +1/R;

at x=2 from +1/R to -1/R;

at x=3 from -1/R to 0;

In configuration 2 there are also discontinuities at locations:

at x=4 from 0 to -0.1/R;

at x=6 from -0.1/R to 0.1/R;

at x=8 from 0.1/R to 0;

Configuration 1 will be used to illustrate the Gibbs phenomenon for splines and the comparison between configurations 1 and 2 to illustrate the properties of the variation of the interpolation error.

Let's consider configuration 1 and assume that the function is sampled at a constant rate and the values of the functions are known at abscissas corresponding to the black dots in Figure 3~~Figure 3~~. Figure 3~~Figure 3~~a, c, e report the comparison between the function $f(x)$ and its cubic spline interpolation $s(x)$ in the region around some of the sections where the curvature discontinuity occurs (x=2, x=3). This comparison clearly shows the oscillation of the spline interpolation around the actual value of the function. The values of the interpolation error, calculated as the absolute value of the difference between the function and its spline interpolation:

$$E(x) = |f(x) - s(x)| \tag{8}$$

are reported in Figure 3~~Figure 3~~b, d, and f for the three sections where there is a discontinuity of the curvature. Due to the oscillations of the interpolating spline function around a discontinuity, the interpolation error reaches the highest values in the two intervals at the sides of the discontinuity and gradually decreases with distance.

Furthermore, the higher the discontinuity of the curvature (for example from -0.1/R to 0.1/R at x=6; that is a discontinuity of the curvature equal to 0.2/R), the higher the absolute value of the interpolation error. This is shown by the comparison between Figure 3~~Figure 3~~d (variation of curvature between configuration 1 and configuration 2 equal to 2/R), and Figure 3~~Figures 3~~b, f (variation of curvature between configuration 1 and configuration 2 equal to ±1/R). The interpolation error can thus be assumed as a 'measure' of the curvature discontinuity since a monotonic relationship holds between the value of the interpolation error $E(x)$ and the discontinuity of curvature. Due to the local character of the spline interpolation, the discontinuity of curvature affects the values of the interpolation only in the region of the curve close to the discontinuity. Therefore, the interpolation error exhibits higher values in a limited region close to the locations where there is a discontinuity in~~of~~ the curvature.

Now consider configuration 2. At the locations where the discontinuity of curvature is equal to the one in configuration 1 (abscissas x=1, x=2 and x=3) the interpolation error does not show any change, as reported in Figure 4~~Figure 4~~a where the values of the interpolation errors relevant to configurations 1 and 2 are compared at location x=2. On the contrary, at the locations where a new discontinuity appears (for example at x=4), the interpolation error increases, as shown by the comparison reported in Figure 4~~Figure 4~~b, between the interpolation errors in the two configurations. Vice versa, if configuration 1 is considered as a modification of configuration 2, a reduction of curvature discontinuity causes a reduction of the interpolation error in the same section (see Figure 4~~Figure 4~~b).

This shows that there is proportionality between the interpolation error and the curvature discontinuity: the increase of the first corresponds to an increase of the second and also a decrease of the interpolation error corresponds to a reduction of the curvature discontinuity.

It is important to underline that herein the assumption of small rotations has been implicitly considered. The relationship between the curvature 1/r and the second derivative of a function is the following:

$$\frac{1}{r} = \frac{\left| f''(x) \right|}{\left| 1 + f'(x)^2 \right|^{\frac{3}{2}}} \tag{9}$$

If the function $f(x)$ represents a deformed shape (as is the case herein), $f'(x)$ is the rotation.

For small values of the rotations, the square of the rotation can be neglected with respect to unity and it can be assumed that the curvature 1/r is equal to the modulus of the second derivative of the function $\left| f''(x) \right|$. A discontinuity in the curvature (1/r) in this case has a direct effect on the second derivative of the function. In the example reported in Figure 2~~Figure 2~~ the assumption of small rotations is well verified at location 1 where the slope of the function $f'(x)$ is zero. At location 2 the function has a vertical tangent so the slope tends to infinity. Therefore the value of curvature at location 2 is still related to the value of the second derivative but the slope effect ~~has a~~ is not negligible~~ effect,~~ therefore they are not equal. As a consequence the values of the interpolation error at location 1 (small rotations) and at location 2 (large rotations) are not comparable.

The assumption of small rotations is commonly valid and adopted to describe the behavior of civil structures therefore the conditions in which the SIM will be applied correspond to those at location 1. In order to clearly show the linear relationship between the values of the interpolation error and of the curvature, in the assumption of small rotation,~~ in~~ Figure 5~~Figure 5~~ ~~are reported~~reports the

values of the interpolation error corresponding to different curvature discontinuities at location 1 (i.e. slope equal to zero).

A slight deviation from this behavior may be observed if a new discontinuity of the curvature appears 'close' to another one. The overlapping of the oscillations of the spline interpolation due to the Gibbs phenomenon may lead, in the region between the two discontinuities, to anomalous variations in~~of~~ the interpolation error. In Figure 6~~Figure 6~~a the variation of the interpolation error E_2-E_1 between configurations 1 and 2 is reported and in Figure 6~~Figure 6~~b a zoom of Figure 6~~Figure 6~~a, limited to the region x=3.4- 4 is reported. Figure 6~~Figure 6~~b shows a decrease of the interpolation error in the region close to the location (x=4) where an increase in~~of~~ the curvature discontinuity occurs. This effect decreases with the spatial resolution (that is the distance between two consecutive knots) of the available data (cfr Figure 7~~Figure 7~~a, b) and also at the increase of the distance between the two sections where the discontinuity of curvature occurs. In any case it causes quite small variations ~~of~~ in the interpolation error with respect to those induced by the curvature discontinuity.

~~Basing~~ Based on all these observations the increase ~~of~~ in the interpolation error can be reasonably used to detect a localized increase ~~of~~ in curvature. A decrease of the interpolation error may be due to a decrease ~~of~~ in the discontinuity of curvature or to the overlap of the Gibbs oscillations (of opposite sign) in the region between two very close discontinuities. In both cases the decrease ~~of~~ in the interpolation error does not denote a reduction of stiffness.

3. THE SURFACE INTERPOLATION DAMAGE DETECTION METHOD

The basic idea of the Surface Interpolation Method can be described with reference to Figure 8~~Figure 8~~. Let (x_0, y_0),…, (x_l, y_p),…, (x_{n_l+1}, y_{n_p+1}), be the instrumented locations of the plate where responses in terms of acceleration have been recorded. At each frequency value, the set of Frequency Response Functions (FRFs) H_R, calculated from measured responses, give the operational deformed shape (ODS) at that frequency.

A localized reduction of stiffness~~,~~ causes a change of the operational shapes in the region close to that location hence this variation can be used to detect the location of damage. The change of the ODS between the undamaged and the damaged configurations can be highlighted by the interpolation of the ODSs through a smooth shape function and by the comparison between the interpolation errors relevant to the (possibly) damaged and the undamaged configurations. In the case of plate-like (that is bi-dimensional) structures, the interpolation of the operating deflection shapes can be carried out using bi-cubic spline functions.

3.1. Estimation of the Interpolation error

Assuming that sensors li~~y~~e on a rectangular grid n_{l+1} x n_{p+1}, for each value of frequency f_i, the actual value $H_R(x_l, y_p)$ of the FRF at a given location (x_l, y_p), and its spline interpolation $H_S(x_l, y_p)$ must be known in order to calculate the value of the interpolation error at that location: $E(x_l, y_p)$, as shown in Figure 8~~Figure 8~~. To this aim the spline interpolation $H_S(x_l, y_p)$ is calculated bas~~ed~~ing on the FRFs at all the instrumented locations except $H_R(x_l, y_p)$.

Actually if only one response is neglected in the interpolation, a non-regular grid is obtained as shown in Figure 9~~Figure 9~~. In order to overcome this problem, two regular grids have been defined, as shown in Figure 10~~Figure 10~~, by neglecting all the responses recorded on one row or on one column of the grid.

Following the two-steps procedure outlined in section 2.2, at each instrumented location the two values of the bi-cubic spline interpolation (one for each of the two grids obtained by removing one row or one column) can be calculated as:

$$H_{S,x}(x, y, f_k) = \sum_{i=0}^{3}\sum_{j=0}^{3} X_{jp,i(l-1)}(f_k)(x - x_{l-1})^i (y - y_p)^j \qquad x_l \in [x_{l-1}, x_{l+1}];\ y_p \in]y_p, y_{p+1}[\quad (10)$$

$$H_{S,y}(x, y, f_k) = \sum_{i=0}^{3}\sum_{j=0}^{3} Y_{j(p-1),il}(f_k)(x - x_{l-1})^i (y - y_p)^j \qquad x_l \in]x_l, x_{l+1}[;\ y_p \in]y_{p-1}, y_{p+1}[\quad (11)$$

For each frequency value f_i, the coefficients, $X_{jp,i(l-1)}$ and $Y_{j(p-1),il}$ are calculated as functions of the H_R measured at all the nodes of the grid except those with $x=x_l$ (for $X_{jp,i(l-1)}$) and except those with $y=y_p$ (for $Y_{j(p-1),il}$).

Bas~~ed~~ing on the two values of the interpolated FRF, at each instrumented location (x_l, y_p) and for each frequency value f_i, two values of the interpolation error E_x and E_y can be calculated:

$$E_x(x_l, y_p, f_k) = \left| H_R(x_l, y_p, f_k) - H_{S,x}(x_l, y_p, f_k) \right| \quad (12)$$

$$E_y(x_l, y_p, f_k) = \left| H_R(x_l, y_p, f_k) - H_{S,y}(x_l, y_p, f_k) \right| \quad (13)$$

The two values of the error E_x and E_y are the values of the interpolation error computed respectively in x and y direction~~s~~. Each of these two features exhibits the properties of the interpolation error in one dimension ~~proved~~ shown in the Appendix of the paper. In other words each of the two values of the interpolation error increases, at the location where it is computed,

proportionally with the curvature discontinuity. The value of the total interpolation error at a given location is given by the sum of the two values in the two directions.

The total interpolation error at the given location can be calculated as the sum of the two latter values:

$$E(x_l, y_p, f_i) = E_x(x_l, y_p, f_i) + E_y(x_l, y_p, f_i) \quad (14)$$

In order to characterize each location $P(x, y)$ (in the following the suffix p and l will be dropped for clarity of notation) with a single error parameter, the norm of the error on the significant frequency range (that is the frequency range with a signal to noise ratio sufficiently high to allow a correct definition of the FRF) is calculated:

$$E(x,y) = \sqrt{\sum_{i=n_o}^{n_o+N} E(x, y, f_i)^2} \quad (15)$$

The significant frequency range is selected limiting the summation in equation (1515) to the frequency range of the fundamental modes of the structure that can be tuned basediing on vibration tests carried out on the undamaged structure. In equation (1515) N is the number of frequency lines in the Fourier transform correspondent to the frequency range starting at line n_o, where the signal to noise ratio is high enough to allow a correct definition of the FRFs.

The values of the transfer functions H_R depend on the state of the structure. Hence, if the estimation of the error function through equation (1515) is repeated in the baseline (undamaged) and in the inspection (possibly damaged) configuration, then the difference between the two values, denoted respectively by $E_0(x,y)$ and $E_d(x,y)$, can provide an indication about the existence of degradation at location (x,y):

$$\Delta E(x,y) = E_d(x,y) - E_0(x,y) \quad (16)$$

Due to the Gibbs phenomenon described in section 2.4, an increase in the interpolation error between the reference configuration and the current configuration at a station $P(x,y)$, i.e. $\Delta E(x,y) > 0$, highlights a localized reduction of smoothness in the vibration amplitude profile.

A positive value of ΔE is thus assumed to be a symptom of a local decrease of stiffness at location $P(x,y)$ associated with the occurrence of damage. Basediing on this assumption the following conditions will be assumed to define the damage index $IDI(x, y)$:

$$\begin{aligned} IDI(x,y) &= \Delta E \quad && if \quad \Delta E(x,y) \geq 0 \\ IDI(x,y) &= 0 \quad && if \quad \Delta E(x,y) < 0 \end{aligned} \quad (17)$$

The first condition ($\Delta E>0$) corresponds to an increase of the interpolation error, that is to a decrease of the smoothness of the amplitude profile. On the contrary, a decrease of the

Formattato: Tipo di carattere: Non Grassetto

Formattato: Tipo di carattere: Non Grassetto

Formattato: Tipo di carattere: Non Grassetto

interpolation error, as shown in section 2.4, may be associated ~~to~~ with an increase ~~of~~ in smoothness or may occur in the region between two damaged sections due to an insufficient spatial sampling. In both cases it is not associated to a local reduction of stiffness hence a negative variation of the interpolation error will be assumed to correspond to a null value of the damage index.

Due to several sources, positive variations of the interpolation error E occur even if no damage is present. In order to remove the effect of these random variations, the statistical variation of this parameter can be studied and a threshold can be defined bas~~ed~~ing on the tolerable value of the probability of false alarm P_f (see ~~reference~~ [18]). The threshold of ΔE can be estimated in terms of the average $\mu_{\Delta E}$ and the variance $\sigma_{\Delta E}$ of the values of ΔE at all the instrumented locations. Assuming a Normal distribution, the threshold ΔE_t can be defined as:

$$\Delta E_t(x,y) = \mu_{\Delta E} + \nu\sigma_{\Delta E} \tag{18}$$

The threshold can be fixed bas~~ed~~ing on a given value of the accepted probability of false alarm assuming the parameter ν as the quantile 1-P_f of the standard normal distribution.

The interpolation damage index (*IDI*) is then calculated as:

$$\begin{aligned} IDI(z) &= \Delta E(z) \quad if \quad \Delta E(z) \geq \Delta E_t(z) \\ IDI(z) &= 0 \quad if \quad \Delta E(z) < \Delta E_t(z) \end{aligned} \tag{19}$$

A localized decrease of stiffness causes a localized increase of curvature that, ~~basing~~ based on the discussion reported in section 2.3~~2.3~~, corresponds to an increase ~~of~~ in the interpolation error.

A decrease of the interpolation error can be related to (i) a localized decrease of curvature (that is to an increase in~~of~~ stiffness or to a limited number of sensors in the region between two discontinuities), or to (ii) ~~to~~ numerical (related to simplifying assumptions in signal processing for example), or to (iii) ~~to~~ experimental errors (related to noise). For these reasons only positive values of ΔE are considered in the evaluation of the damage index *IDI*.

The probability of false alarm P_f is the value accepted for the probability of assuming that the structure is damaged while it is not or, in other words, is the probability that the variation of the interpolation error exceeds the threshold when the structure is still undamaged. In this case the location (x, y) will be wrongly assumed as damaged and a 'false alarm' will be given. The probability P_f is represented by the pointed area under f_{Eo} at the right of the threshold in Figure 11~~Figure 11~~. It must be noted that a second type of error can arise in the case the threshold is not exceeded but the structure is damaged. In this case the alarm will not be given even if the structure is damaged, that is a 'missing alarm' will occur. The 'probability of missing alarm' is represented by the hatched area under f_{Ed} at the left of the threshold in Figure 11~~Figure 11~~.

Formattato: Inglese (Stati Uniti)

Based~~ing~~ on the dispersion of the distributions, different results will correspond to a given choice of P_f . For example, for very noisy signals (hence a~~n~~ high variance of the distribution), a given value of P_f will lead to a higher value of the threshold, with respect to the case of high quality, low noise sensors). ~~hence~~ This leads to a higher value of the probability of missing alarms P_m. Similarly, an increase in P_f will reduce the value of the threshold together with the probability of missing alarms P_m.~~.~~

The choice of the threshold is thus a tradeoff between the probability of false and missing alarm and its choice must be the object of preliminary analysis based on both the condition of testing (quality ~~sensors~~ of the sensors for example, or possible variations ~~of~~ in ambient parameters) and on the consequences of the two types of error. If a false alarm is considered too expensive, from any point of view, then a high value of the threshold is appropriate. On the contrary, if the consequences of a false alarm are not really a problem while the consequences of a missing alarm can be very serious, in this case a low value of the threshold should be chosen.

The choice of the threshold is based~~ing~~ on a cost-benefit analysis and is beyond the scope of this paper, and therefore will not be performed for the application reported in the following section.

4. NUMERICAL EXAMPLES

In order to compare the results given by the SIM with results obtained using another data-driven damage localization methods proposed in literature, the proposed method has been applied to the case of concrete plates proposed in references [15] and [16]. In these papers damage identification was carried out via the uniform load surface method, that uses ~~as a damage feature~~ the modal deflection under a uniform unit load pattern as a damage feature. The SIM has been applied to the same examples in order to show its capability of obtaining the same results without the need ~~of~~ for a previous modal analysis. ~~that is with~~This means is has a lower computational effort. The Uniform load surface method requires ~~the~~ knowledge of modal parameters therefore a modal analyses has to be performed in order to retrieve them ~~from the e.g.~~using, for example, ~~the~~ Frequency Response Functions. On the contrary the SIM uses the operational shapes as input data that can be retrieved fro~~or~~m the Frequency Response Functions without any further computation.

The size of the plates is 420mm x 320mm with a thickness of 20mm. A finite element model of 7x10 plate elements has been built in SAP2000 [26] and reported in Figure 12~~Figure 12~~. The two plates differ for the boundary conditions: the first one is clamped along the edge AB; the second one is supported on the four corners A, B, C, D and with free boundary conditions at all the other boundary joints. A total of 88 four node~~s~~d "area" elements 1m x 0.40mm x 0.20cm are used to

model the plate. The material has a Young's modulus in the undamaged configuration equal to 25000MPa, a Poisson's ratio ν=0.3 and a mass density ρ=2800kg/m^3.

Damage has been modeled by reducing the Young's modulus in the elements located where the development of damage is more likely to occur. ~~Namely f~~For the clamped plate damage has been assumed to be located along the clamped edge in Damage scenario 1 and at one corner in Damage scenario 3. ~~and f~~For the supported plate damage has been considered located around the middle span.

The labels of the damaged elements and the relevant reductions ~~of~~ in Young's ~~modulus~~ moduli are reported in Table 1. Figure 12~~Figure 12~~ and Figure 7 report their positions.

The time history response of the two plates to a random acceleration applied at supports, have been calculated both in the undamaged and in the damaged configurations, assuming a linearly elastic behavior.

The responses in terms of absolute accelerations have been used, together with the random excitation at supports, to calculate the ~~frequency response functions (~~FRFs~~)~~ at all the nodes of the plates and, following the procedure described in section 2, the interpolation error E in the undamaged and in the damaged configurations has been calculated at each node. The interpolation error has been calculated extending the summation of equation (15~~15~~) to the range of frequencies 0-5000Hz where the fundamental modes of the plate l~~y~~ive as shown in Figure 14~~Figure 14~~.

Formattato: Tipo di carattere: Non Grassetto

5. RESULTS

Results for scenarios 1 to 4 are reported in Figure 15~~Figure 15~~ to Figure 19~~Figure 19~~. These results have been obtained assuming that responses are not affected by noise: the noise to signal ratio is nsr=0.1%. In the application of equation (18~~18~~) the parameter ν has been assumed equal to 1 (corresponding to a tolerable probability of false alarms P_f=15%) for damage scenarios 1 and 2 where damage of low intensity (15%) is present. Lower values of this parameter, corresponding to higher values of the threshold $\Delta E_t(z)$, lead to missing alarms at the locations of lower damage.

Formattato: Tipo di carattere: Non Grassetto

For the other damage scenarios (3 and 4), where the minimum stiffness reduction is 25%, the value ν=2 (P_f=3%) allows the correct detection of damage at all locations and no missing alarms occur~~s~~. The peaks of function IDI are correctly located at the nodes of the damaged elements clearly indicating the correct location of damage. The relative height of the peaks correspond~~s~~ to the reduction of stiffness: a higher peak corresponds to more severe damage. This suggests the possibility to upgrade the SIM to a damage identification method of level 3 able to detect, localize

and also quantify damage. At the moment the relationship between the amount of damage and the value of the damage feature has not yet been established ~~yet~~.

For damage scenarios that are usually difficult to detect, such as damage concentrated at one corner (scenario 3) or at two very close locations (scenario 4), the method allows the correct location of damage be established. For the case wherer ~~(~~ν=2 and~~,~~ P_f=3%~~)~~ no false alarm occurs but there is a missing alarm at location 7 (25% reduction of stiffness) for scenario 3; if the probability of false alarm is raised to 15% (ν=1) all damaged locations are correctly detected but a number of false alarms occur~~s~~ (Figure 18~~Figure 18~~).

A last comment regarding~~s~~ the identification of extension of the damaged area is discussed herein. ~~Basing~~ Based on the available sensor~~s~~ layout the method allows locating the nodes of the grid that are closer to the damaged portion of the structure. A finer grid with a greater number of nodes - hence of recording sensors - allows a more precise definition of the damaged area. When designing the monitoring system a reasonable balance between the requirements of precisely detecting the damaged portion of the structure and the need to reduce the cost of the monitoring system should be sought. In order to show the effect of a coarser mesh on the capabilities of the SIM, Figure 28~~Figure 27~~ reports the results relevant to damage scenarios 3 and 4. These scenarios were obtained using a grid of 30 sensors instead of 99 as in the previous figures. The method is still able to localize the region of the plate where damage is but with a much lower resolution.

6. EFFECT OF MEASUREMENT NOISE

Noise in experimental data is one of the major problems for almost all damage detection algorithms since it is one of the principal sources of false or missing detections of damage thus reducing the reliability of results. In order to check the influence of noise on the SIM, artificial noise has been added to responses calculated by the numerical model.

As explained in detail in section 2.3~~2.3~~ the SIM does not need the estimation of curvatures through differentiation because the losses of stiffness are identified as discontinuities of a smooth cubic spline function. This reduces the sensitivity of the algorithm to noise that, on the contrary, limits the reliability of other damage identification methods proposed in literature (see references [9], [11] [12], [14]-[15]). In order to check the sensitivity ~~to noise~~ of the surface interpolation method to noise, responses of the numerical model of the plate have been corrupted with a Gaussian zero mean white noise assuming a noise to signal ratio of 10%. Figure 20~~Figure 20~~ and Figure 21~~Figure 21~~ report the results for the clamped plate: damage scenarios 1 and 3. In both cases all damage locations are correctly detected without any false or missing alarm. The only difference with respect to the case of very low noise is the slightly lower value of the *IDI* at the damaged locations.

Formattato: Tipo di carattere: (asiatico) Giapponese, (Altro) Inglese (Stati Uniti), Crenatura 10 pt

On the contrary, for the supported plate (scenarios 2 and 4) as shown in Figure 22~~Figure 22~~, a value ν=1 leads to a great number of false alarm. Increasing the threshold to ~~(~~ν=2~~,~~ (P_f=3%) all the false alarms, except one at location 6, disappear (see Figure 23~~Figure 23~~)~~,~~ ~~but~~ However, there ~~is~~ remains a missing alarm at location 28, the location less damaged among the three in scenario 2. The same occurs for damage scenario 4. In this latter case, in order to remove the false alarm at location 6 a value P_f=1% has been assumed. As explained in 3.1~~3.1~~ the choice of the value of Pf is beyond the scope of this paper; herein the values chosen for the numerical examples are aimed to show the consequences of the different choices of this probability.

Another remark should be done to explain the missing alarms occurring in the case of ~~multiple~~ damage~~s~~ at different locations and with multiple severities: they depend on the averaging related to the estimation of the threshold through equation (18~~18~~). This effect can be removed if, as for the case reported in reference [16] the distribution of the interpolation error at each location is known in the original configuration and a different value of the threshold is defined for each location. As a matter of fact, in the case of a single damaged element with a small (15%) reduction of stiffness, (scenario 5: only one damaged element at one location) the method is able to detect the correct location of damage also for high level of noise (see Figure 26~~Figure 26~~). In this case the detection is not hampered by the averaging related to equation (18~~18~~), ~~being~~ in that the damaged ~~location~~ location is the only one with a high value of the damage index. As shown by the previous results, the most sensitive issue in the application of the method appears to be the definition of the threshold that selects the locations that are 'truly' damaged from the ones where the variation of the interpolation error is due to other random sources.

The higher the level of noise, the higher should be the threshold in order to avoid false alarms. Of course this limits the ability to detect small amounts of damage hence, in any case, the acquisition of high quality signals with a low noise to signal ratio plays a key role in the increase ~~of~~in the reliability of results and must be a central issue for this, as well as for many other~~s~~, damage identification methods.

7. EXPERIMENTAL VERIFICATION

The accuracy of the proposed surface interpolation method was experimentally assessed by impact hammer tests on a glass fiber/vinylester composite plate of dimensions 500cm x 500cm with thickness 1cm. For the measurement of the responses the plate was divided by a grid of 0.5cmx0.5cm corresponding to 10x10 nodes (see Figure 26). It is noted that the experimental tests were carried out on specimens that differ from the plate considered for the numerical verification of the SIM that, as already remarked in section 4, was chosen in order to compare the results of the

Formattato: Tipo di carattere: (asiatico) Giapponese, (Altro) Inglese (Stati Uniti), Crenatura 10 pt

Formattato: Tipo di carattere: Non Grassetto

Formattato: Tipo di carattere: Non Grassetto

SIM with those given by another method of damage identification, namely the uniform load surface method.

The plate was suspended with a bungee cord to approximate free-free boundary conditions and subjected to a pulse load applied at each point on the grid by an Impulse hammer. Responses in terms of acceleration wasere recorded in all the nodes of the grid and the Operational Deformed Shapes were determined as Frequency Response Functions between each grid point and the reference one. These were determined by averaging those obtained from three impacts at each point. The plate was tested before and after a damage was simulated by manufacturing a flaw at the location shown in Figure 29Figure 27 with an area of about 1.5 x 1.5 cm and a depth of 0.6cm. For the application of the SIM the probability of false alarm has been assumed equal to 2% (ν=2 in equation (1818)) and the frequency range for the application of the SIM, basing based on the FRF measured in the undamaged configuration was chosen to include the frequency range of the fundamental modes of the plate (see Figure 30Figure 28). More details can be found in reference [20].

Formattato: Tipo di carattere: Non Grassetto

In Figure 31Figure 29 the results of the application of the SIM are reported showing that the damaged location is correctly detected by the damage index that exhibits the highest values at the four nodes of the damaged elements. Due to the interpolation process [17] some false alarms are found at locations close to the damaged ones. Even if this it can reduce the precision in the identification of the contour of the damaged area, it does not hamper its correct localization since it affects only locations adjacent to the damaged one.

In some cases damage can be manifest itself as a crack or as a delamination and this leads to a jump of the first derivative of the function (see for example references [28] and [29]). In this paper, it was proved that a discontinuity of in stiffness (proportional to the second derivative) induces a jump in the interpolation through a spline function. This type of interpolation imposes the continuity of the first derivative as well as of the second. Therefore an increase of the interpolation error is expected also at locations where a discontinuity of the first derivative occurs due to, for example, a crack. This means that in principle the method can detect discontituities of the first derivative as well as of the second derivative. However this requires future further research efforts in order to assess the potentiality of the method for practical applications.

8. CONCLUSIONS

In this paper has been proposed, extension of the Surface Interpolation Method (SIM) to plate-like structures has been proposed, as the Surface Interpolation Method (SIM), the extension to plate

~~like structures of the Interpolation Method previously proposed by the author~~. In order to compare the performance of the SIM to ~~an~~other damage localization method~~s~~, it has been applied herein to the case of the concrete plates proposed in references [15] and [16]. Experimental tests have also been ~~also~~ carried out on a composite plate to verify the practical application of the proposed algorithm. Results indicate that the method is a viable method for damage localization with the advantage, providing with respect to other method~~s~~ proposed in literature, that the same accuracy in damage localization is desired with a lower computational effort. Advances in sensor~~s~~ technology and miniaturized signal processing platforms allow ~~exploring~~ exploration of the possibility of realizing an autonomous monitoring system based on responses recorded by a large number of sensors widely distributed over a~~the~~ structure. From this point of view the minimum interaction with a human operator required by the SIM makes it appealing for automatic damage detection through a permanent monitoring system integrated with a data processing software.

AKNOWLEDGEMENTS

The author wishes to thank Valter Carvelli and Marco Cucchi of Politecnico di Milano for their help and assistance with the experimental tests.

APPENDIX

In this Appendix it is proved that when a function having a jump discontinuity in its second derivative is approximated by a cubic spline function, an 'overshoot' effect occurs on each side of the discontinuity. The overshoot is proportional to the size of the jump.

The proof is based on the Corollary 2 of Theorem V.1 [1] and on the demonstration given in reference [2] of the existence of the Gibbs phenomenon for piecewise linear functions that are briefly recalled for the sake of completeness.

According to the Corollary 2 of Theorem V.1 [1] the second derivative *s''* of the complete spline *s* interpolant to the function *g*, is the least square approximation from the space of piecewise linear interpolants to the second derivative of *g*.

This means that when a function *g* is interpolated with a cubic spline *s*, the second derivative *s*'' (which is a piecewise linear function) approximates the function *g*''(*x*) in the least square sense that is, it satisfies the following relationship:

$$\int_a^b \left[s''(x) - g''(x) \right]^2 dx = \min \qquad \text{(A1)}$$

In reference [2] is proved that an analog of the Gibbs phenomenon (overshoot that occurs when a jump-discontinuous function is approximated in the least square sense) holds for piecewise linear approximations and the maximum overshoot is equal to 0.26794919 multiplied by one-half the magnitude of the jump.

Proof

Assume we have a function $g(x)$ with a jump c in its second derivative $g''(x)$ and we want to approximate $g(x)$ with a cubic spline $s(x)$. ~~See~~ see Figure 32~~Figure 30~~.

For simplicity of notation let's put:

$$y(x) = s''(x) \tag{A2}$$

Without loss of generality, following the procedure proposed in reference [2] let's assume a simple step function for $g''(x)$:

$$g''(x) = \begin{cases} -c & -1 < x < 0 \\ +c & 0 < x < 1 \end{cases} \tag{A3}$$

Given interpolating points $-1 = x_{-n} < x_{-n+1} < \ldots x_{-1} < x_0 < x_1 < \ldots x_{n-1} < x_n = 1$ we want to construct a piecewise linear function $y(x)$ that best approximates $g''(x)$ in the least squares sense that is:

$$\int_{-1}^{0} \left[y(x) + c \right]^2 dx + \int_{0}^{1} \left[y(x) - c \right]^2 dx = \min \tag{A4}$$

and with boundary conditions $y(x_{-n}) = 0$, $y(x_n) = 0$.

Our unknowns are the values of function y in the nodes x_k, $k = -n+1, \ldots, n-1$.

Taking into account the symmetry of the function $g''(x)$, that requires the symmetry of the interpolant on the two sides of the jump $y(x_k) = y(-x_k)$, the solution of equation (A4) can be found by solving the following:

$$\int_{0}^{1} \left[y(x) - c \right]^2 dx = \min \tag{A5}$$

Symmetry also requires that $y(x_0) = 0$ so our unknowns reduce to the $n-1$ values $y_1, \ldots, y_{n-1}$ that minimize equation (A5).

Let's assume that the knots are equally spaced and indicate with $\Delta x = 1/n$ the distance between two successive knots.

Commentato [LP-C1]: Nodes?

Being $y(x)$ a linear function, in the generic interval $x_k \le x \le x_{k+1}$, ($x_k = k\Delta x$ k=0, 1, 2,…, n), the following relation holds:

$$\frac{y(x)-y_k}{y_{k+1}-y_k} = \frac{x-x_k}{x_{k+1}-x_k} \tag{A6}$$

where $y_k = y(x_k)$ is the value of the interpolant at knot x_k.

Rearranging, substituting $x_k = k\Delta x = k/n$ and subtracting 1 on both sides we obtain:

$$y(x)-c = (nx-k)(y_{k+1}-y_k)+y_k-c \tag{A7}$$

Let's indicate with:

$$w_k = y_k - c \tag{A8}$$

the overshoot at knot k that is the difference between the value of the function c and the value of the interpolating function y_k.

Substituting w_k in the previous expression:

$$y(x)-c = (nx-k)(w_{k+1}-w_k)+w_k \tag{A9}$$

$$\int_{x_k}^{x_{k+1}} \left[y(x)-c\right]^2 dx = \frac{1}{3n}\left(w_{k+1}^2 + w_{k+1}w_k + w_k^2\right) \tag{A10}$$

Equation (A7) can thus be written as:

$$\int_0^1 \left[y(x)-c\right]^2 dx = \frac{1}{3n}\left(2\sum_{k=1}^{n-1} w_k^2 + \sum_{k=1}^{n-2} w_{k+1}w_k + w_n^2 + w_0^2 + w_1w_0 + w_nw_{n-1}\right) \tag{A11}$$

In our case:

$$w_n = 0-c = -c,\ w_0 = 0-c = -c, \tag{A12}$$

thus:

$$\int_0^1 \left[y(x)-c\right]^2 dx = \frac{1}{3n}\left(2\sum_{k=1}^{n-1} w_k^2 + \sum_{k=1}^{n-2} w_{k+1}w_k + 2c^2 - cw_1 - cw_{n-1}\right) \tag{A13}$$

Imposing that the partial first derivative with respect to all w_k (k=1,…n-1) vanish, we obtain a system of equation in the unknowns $w_1,...w_{n-1}$:

$$\begin{cases} 4w_1 + w_2 = c \\ w_{k-1} + 4w_k + w_{k+1} = 0 & 2 \le k \le n-2 \\ w_{n-2} + 4w_{n-1} = c \end{cases} \tag{A14}$$

The general solution is:

$$w_k = c_1\lambda_1^k + c_2\lambda_2^k \tag{A15}$$

with λ_1 and λ_2 solutions of the characteristic equation:

$$\lambda^2 + 4\lambda + 1 = 0 \qquad \lambda_{1/2} = -2 \pm \sqrt{3} \tag{A16}$$

and the constants c_1 and c_2 determined from equation (A15) by the initial conditions ($w_o = w_n = -c$):

$$c_1 = -c \cdot \frac{\left(\lambda_2^n - 1\right)}{\left(\lambda_2^n - \lambda_1^n\right)} \qquad c_2 = c \cdot \frac{\left(\lambda_1^n - 1\right)}{\left(\lambda_2^n - \lambda_1^n\right)} \tag{A17}$$

The general solution is:

$$w_k = -c \cdot \frac{\left(\lambda_1^k + \lambda_1^{n-k}\right)}{\left(1 + \lambda_1^n\right)} \quad \text{with} \qquad \lambda_1 = -2 + \sqrt{3} \cong -0.268\,; \tag{A18}$$

Let's investigate how the overshoot w_k varies at the increase of the distance from the jump (k=0) that is at the increase of k.

The difference between the (positive) values of the overshoot at two consecutive knots k and k+1 is the following:

$$(-1)^{k+1} w_k - (-1)^{k+2} w_{k+1} = c \cdot (-r_1)^k (r_1 + 1) \frac{\left(r_1^{n-2k-1} + 1\right)}{\left(1 + r_1^n\right)} \tag{A19}$$

This difference is positive for $1 \le k < n/2$ therefore the maximum value of the overshoot w_k occurs at k=1 that is at the location of the jump and its value is:

$$w_1 = -c \cdot \frac{\left(\lambda_1 + \lambda_1^{n-1}\right)}{\left(1 + \lambda_1^n\right)} = -c \cdot \frac{\left(-0.268 + 0.268^{n-1}\right)}{\left(1 + 0.268^{n-1}\right)} \tag{A20}$$

This proves that when a cubic function is utilized to interpolate a function with a jump c, the value of the overshoot is proportional to the magnitude of the jump c.

At the increase of the number of knots n the value of the overshoot decreases but does not vanish and its limit value is:

$$\lim_{n \to \infty} w_1 = 0.268 \cdot c \tag{A20}$$

This overshoot (see equations A8 and A2) is the difference between the second derivatives of the interpolant function $s(x)$ and of the function $g(x)$.

$$\lim_{n \to \infty} w_1 = \lim_{n \to \infty} (y_1 - c) = \lim_{n \to \infty} \left(s''(x_1) - g''(x_1)\right) = 0.268 \cdot c \tag{A21}$$

This value corresponds to the second derivative of the interpolation error $E(x) = s(x) - g(x)$, at the location $x = x_1$ of the discontinuity *c* of the second derivative.

[1] de Boor C. "*A Practical Guide to Spline*". Springer Verlag, New York, N.Y., 1978.

[2] Foster J., Richards F.B. (1991). The Gibbs Phenomenon for Piecewise-Linear Approximation. *The American Mathematical Monthly*, Vol. 98, No. 1. pp. 47-49.

[3] J. Willard Gibbs, letter to the editor, *Nature* 59 (April 27, 1899) 606.

9. REFERENCES

1. Ho Y.K., Ewins D.J. "On the structural damage identification with mode shapes". *Proc. of the European COST F3 Conference on Structural Identification and Structural Health Monitoring*. Madrid, Spain 2000, 677-686.
2. Pandey A.K., Biswas M., Samman M.M. (1991). "Damage detection from change in curvature mode shapes". *Journal of Sound and Vibration*, 145 (1991), pp. 321–332.
3. Ciambella J., Vestroni F. (2015). "The use of modal curvatures for damage localization in beam-type structures". *Journal of Sound and Vibration*, 340, pp. 126-137.
4. Dilena, M., Morassi, A., Perin, M. 2011. Dynamic identification of a reinforced concrete damaged bridge. *Mech. Syst. Signal Pr.* 25(8), p. 2990–3009.
5. Kim J.T., Stubbs N. (2002). "Improved damage identification method based on modal information" *Journal of Sound and Vibration*, 252 (2002), pp. 223-238.
6. Zhang, Z., Aktan, A.E. *(* 1998*)*. Application of modal flexibility and its derivatives in structural identification. *Research in Nondestructive Evaluation* , 10, 43-61.
7. Fan W., Qiao P., (2011). "Vibration-based Damage Identification Methods: A Review and Comparative Study". *Structural Health Monitoring*", 10(1): 83–29.
8. Ratcliffe C.P., (2000). A frequency and curvature based experimental method for locating damage in structures. Transactions of the American Society of Mechanical Engineers. *Journal of Vibration and Acoustics*, 122: 324–329.
9. Sampaio R.P.C., Maia N.M.M., Silva J.M.M., (1999). Damage detection using the frequency response function curvature method. *Journal of Sound and Vibration*, 226(5): 1029 1042.
10. Limongelli, M.P., (2010). Frequency Response Function Interpolation for Damage Detection under Changing Environment. *Mechanical Systems and Signal Processing*, 24(8), 2898-2913.
11. Zhang Y., Xiang. (2011). 'Frequency shift curve based damage detection method for beam structures'. Computers, Materials & Continua, 26 (1), pp. 19–35.

Formattato: Olandese (Paesi Bassi)

12. Cornwell P., Doebling S.W., Farrar,C.R., (1999), "Application of the strain energy damage detection method to plate-like structures,'' *Journal of Sound and Vibration*. 224, pp. 359–374.
13. Yoon M.K., Heider D., Gillespie, J.W., Ratcliffe C.P., Crane R. M. (2005). Local damage detection using the two-dimensional gapped smoothing method. *Journal of Sound and Vibratio*n. Vol 279, 119 139.
14. Zhang Y., Wang L., Lie S. T., Xiang Z.H. (2013) "Damage detection in plates structures based on frequency shift surface curvature''. *Journal of Sound and Vibration*. 332(25), pp. 6665–6684.
15. Wu D. Law S.S. (2004). Damage localization in plate structures from uniform load surface curvature. *Journal of Sound and Vibration*, 276: 227 244
16. D. S.S. Law (2005). Sensitivity of Uniform Load Surface Curvature for Damage Identification in Plate Structures. Transactions of the American Society of Mechanical Engineers. Journal of Vibration and Acoustics, 127: 84–92.
17. Limongelli, M.P., (2011). The interpolation damage detection method for frames under seismic excitation. Journal of Sound and Vibration, 330. 5474–5489.
18. Limongelli, M.P., (2014). Seismic health monitoring of an instrumented multistorey building using the Interpolation Method. Earthquake Engng. Struct. Dyn. doi: 10.1002/eqe.2411
19. Limongelli M.P., Domaneschi M., Martinelli L., (2016). Vibration-based damage severity estimation basing on a non-model damage feature. IALCCE 2016. Delft, The Netherlands
20. The modal surface interpolation method for damage localization. *12th International Conference on Damage Assessment of Structures*. IOP Conf. Series: *Journal of Physics: Conf. Series* 842. 012004 doi :10.1088/1742-6596/842/1/012004
21. Hou H.S., Andrews H.C.. (1978), "Cubic Splines for image Interpolation and Filtering". *IEEE Transactions on Acoustics, Speech, and Signal Processing*, 26(6), 508-517.
22. C.de Boor. (1978). "A Practical Guide to Spline". Springer Verlag, New York, N.Y. 1978.
23. Zhan Z., Martin C.F. (1997). "Convergence and Gibbs' phenomenon in cubic spline interpolation of discontinuous functions*".* Journal of Computational and Applied Mathematics 87, 359-371.
24. Long S., Zhang T., Long F. (2005), 'Causes and solutions of overshoot and undershoot and end swing in Hilbert-Huang transform'. *Acta seismologica Sinica*, 18, 602-610.
25. Richards F.B. (1991), 'A Gibbs phenomenon for Spline Functions' Journal of Approximation Theory, 66, 344-351.
26. "SAP2000." Computer and Structures Inc.

27. Rytter, A., 1993. *Vibration Based Inspection of Civil Engineering Structures*. PhD Thesis. Aalborg University, Denmark.
28. N. Corrado, M. Gherlone, C. Surace, J. Hensman, N. Durrande, Damage localisation in delaminated composite plates using a Gaussian process approach, Meccanica, 50 (10), 2537-2546, 2015.
29. C. Surace, R. Saxena, M. Gherlone, H. Darwich, Damage localisation in plate like-structures using the two-dimensional polynomial annihilation edge detection method, Journal of Sound and Vibration 333(2014) 5412-5426

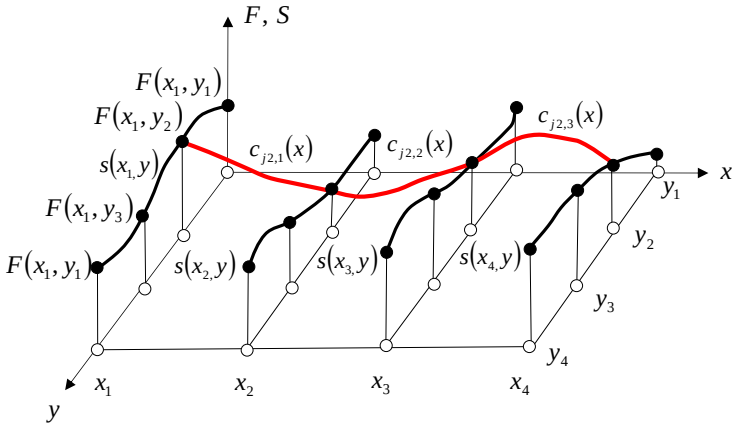

Figure 1. Bi-cubic spline interpolation

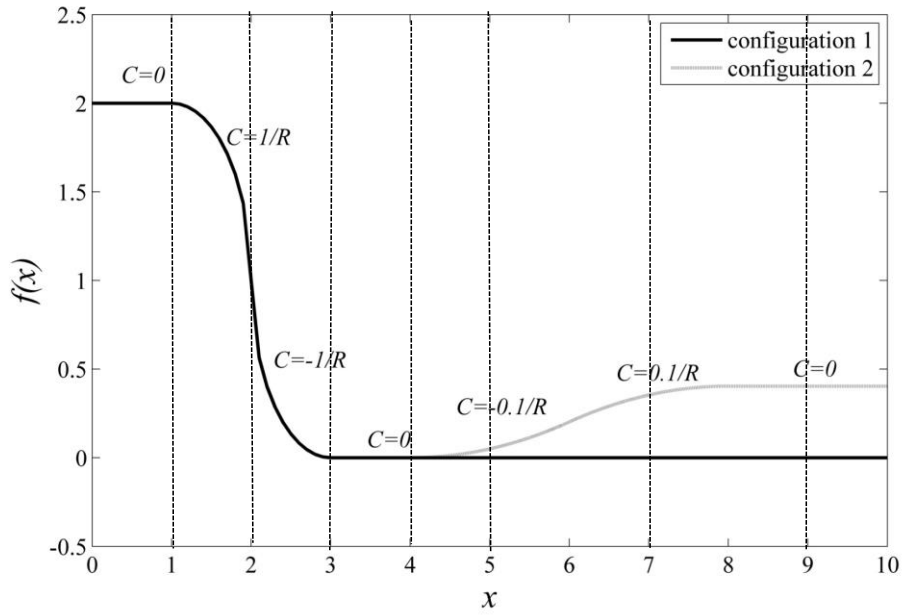

Figure 2. Two different configurations of a curve with localized discontinuities of curvature

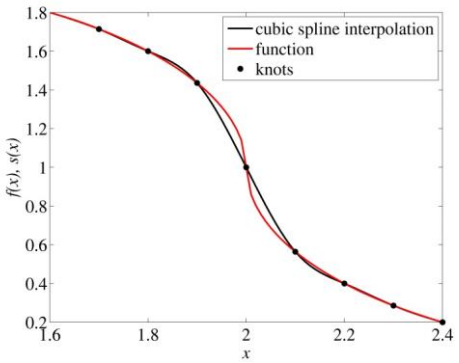

(c)

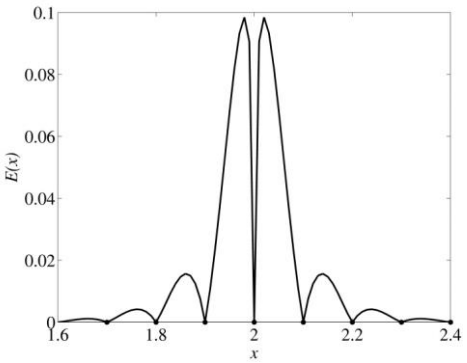

(d)

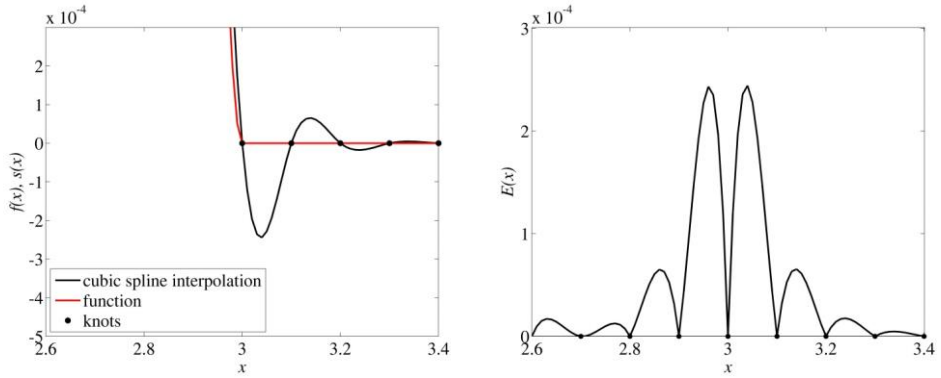

(e) (f)

Figure 3. Gibbs phenomenon of splines

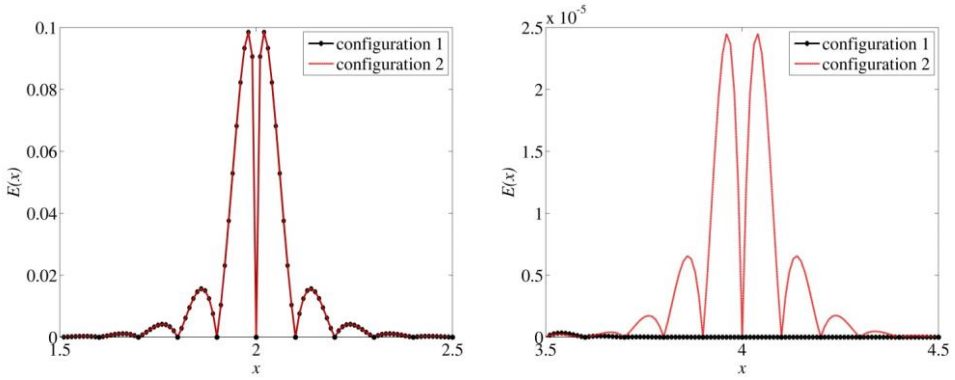

(a) (b)

Figure 4. Comparison of interpolation error in two configurations a) equal discontinuity of curvature in configurations 1 and 2 at location x=2; b) increase of discontinuity of curvature in configuration 2 with respect to configuration 1 at location x=4.

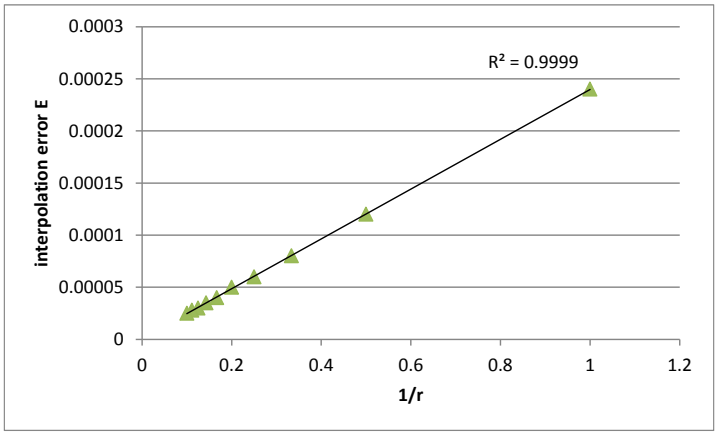

Figure 5. Variation of the interpolation error with the curvature for location 1 in Figure 2~~Figure 2~~.

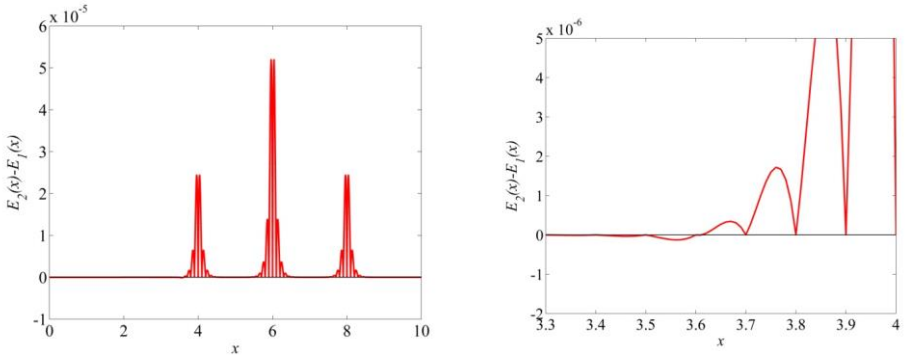

(a) (b)

Figure 6. Decrease of the interpolation error in the region between two discontinuities of curvature ($3<x<4$).

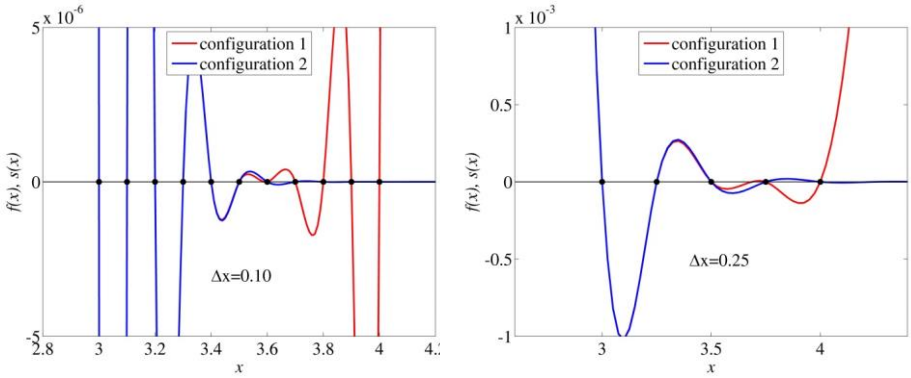

(a) (b)

Figure 7. Variation of the interpolation error with spatial resolution of sensors.

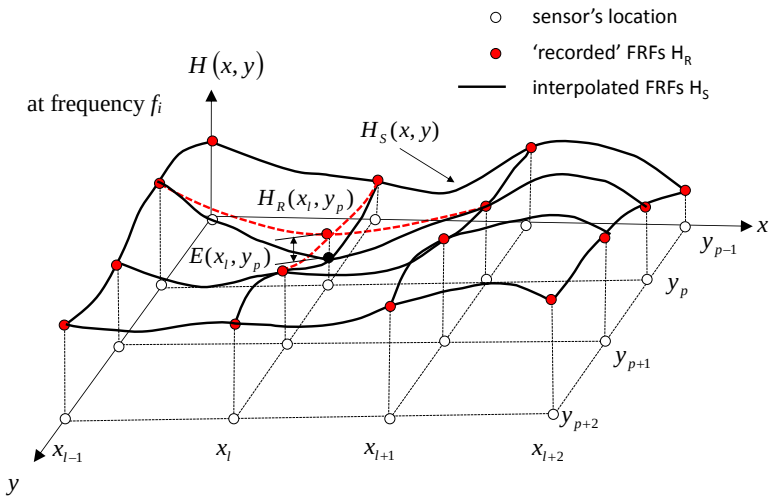

Figure 8. The interpolation error $E(x,y)$

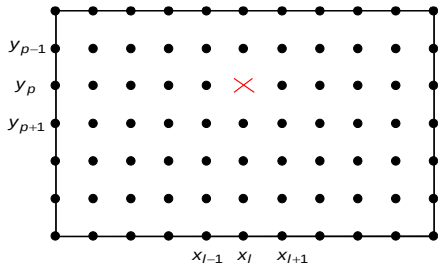

Figure 9. Grid of knots for the interpolation at location P(x_l, y_p)

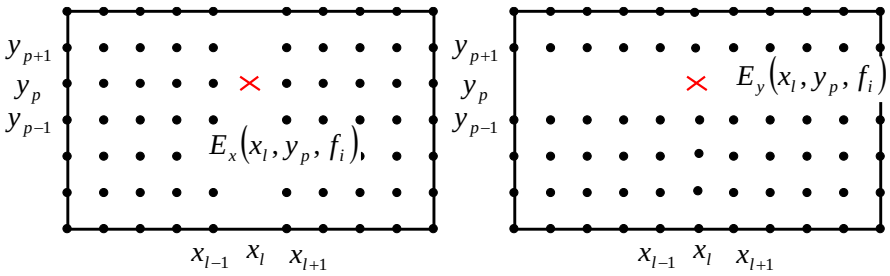

Figure 10. Regular grids for the evaluation of the interpolation error

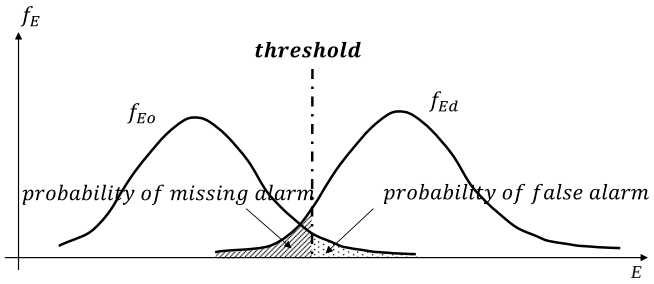

Figure 11. Probability of false and missing alarm

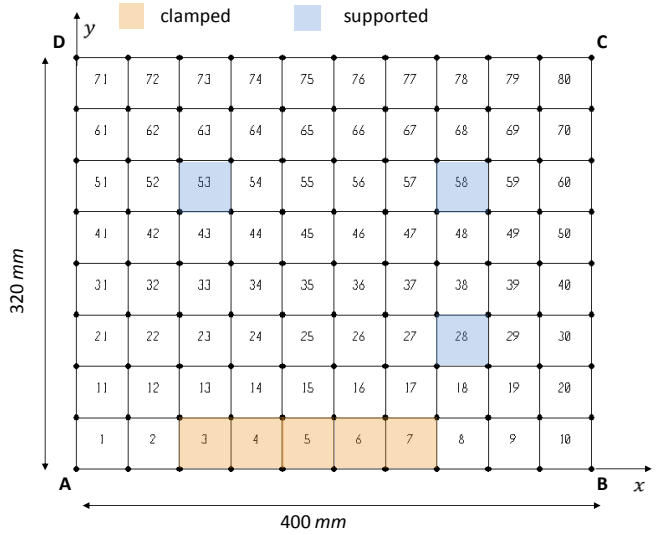

Figure 12. Numerical model of the plate and damage scenarios 1 and 2. Grid of 99 sensors

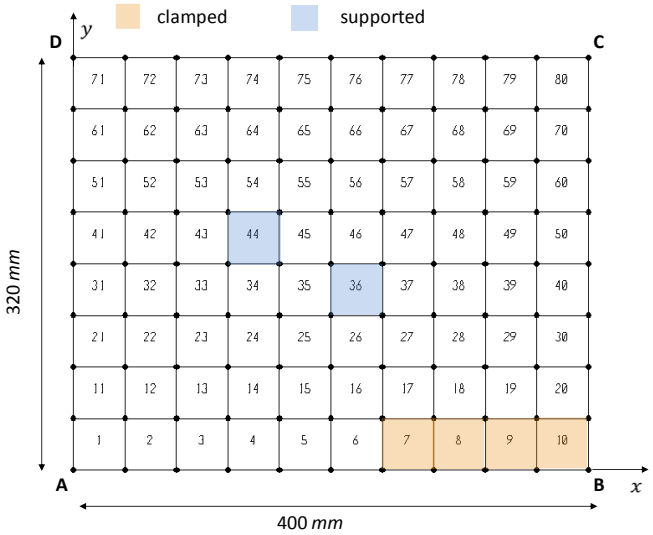

Figure 13. Damage scenarios 3 and 4

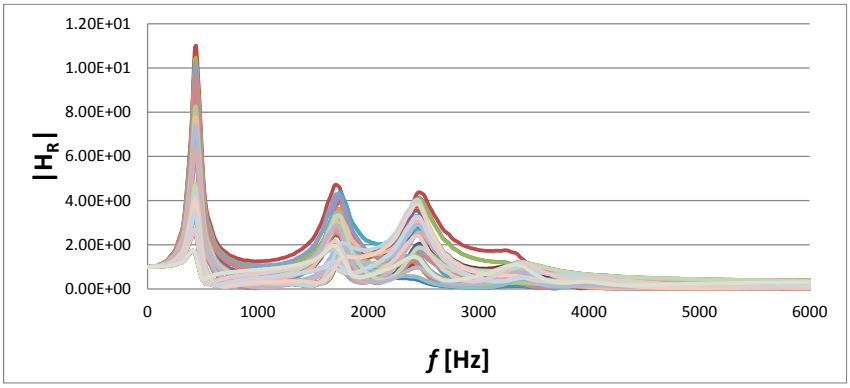

Figure 14. Magnitude of FRFs at the nodes of the plate

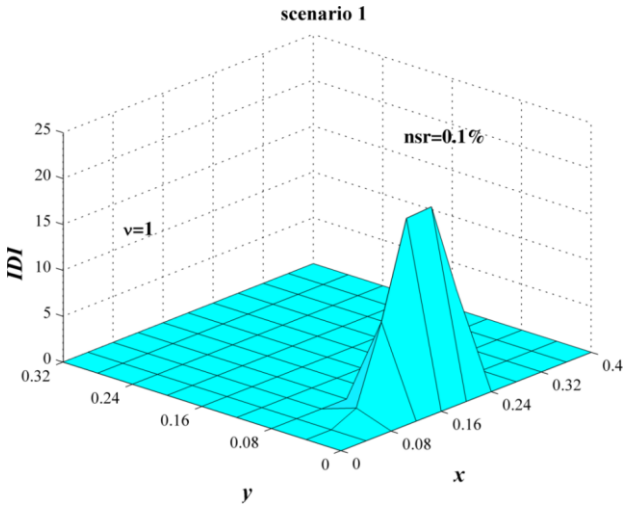

Figure 15. Results for scenario 1: *nsr* =0.1%

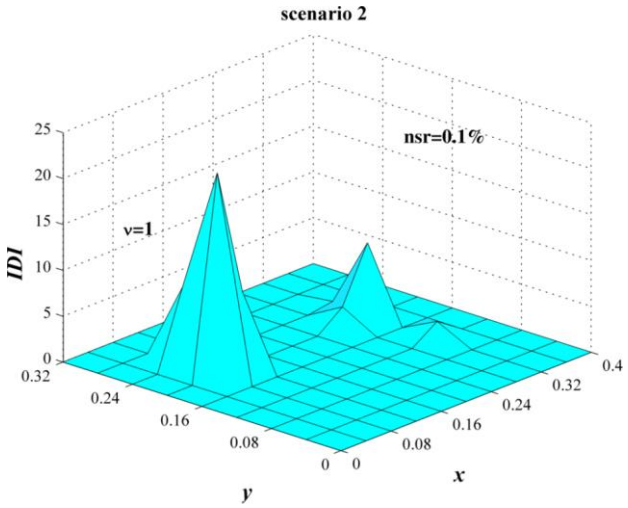

Figure 16. Results for scenario 2: *nsr*=0.1%

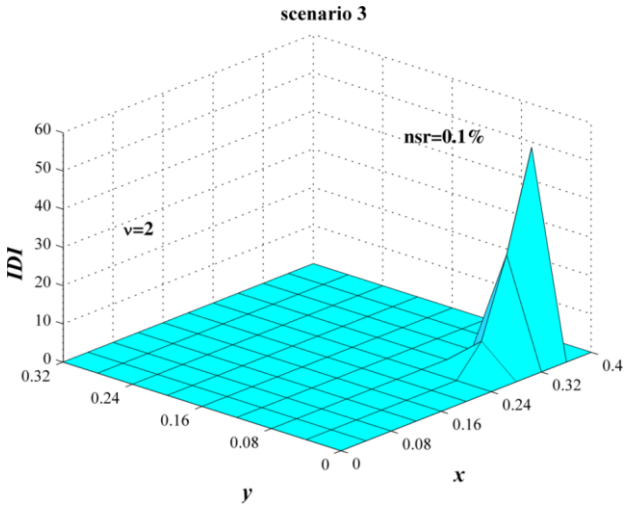

Figure 17. Results for scenario 3: *nsr* =0.1%, P_f=3%

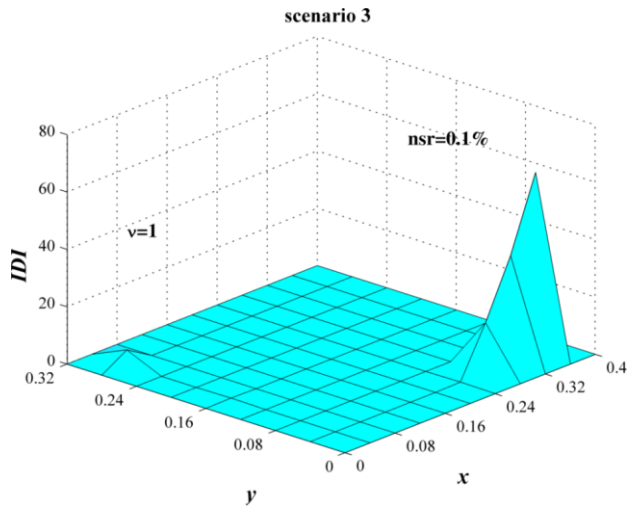

Figure 18. Results for scenario 3: *nsr* =0.1%, P_f =15%

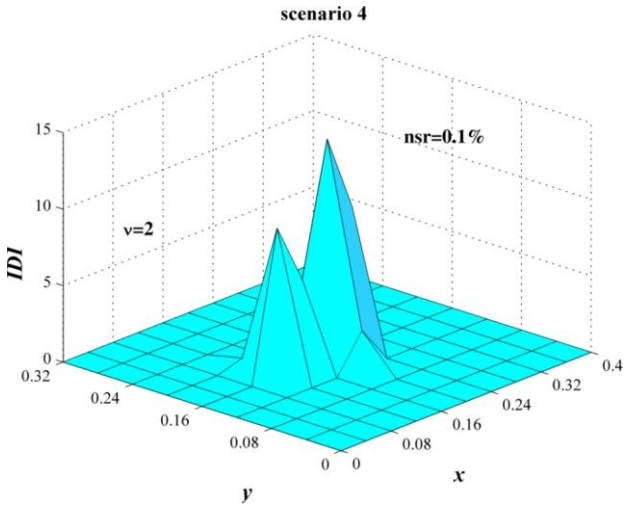

Figure 19. Results for scenario 4: *nsr* =0.1%, P_f=3%

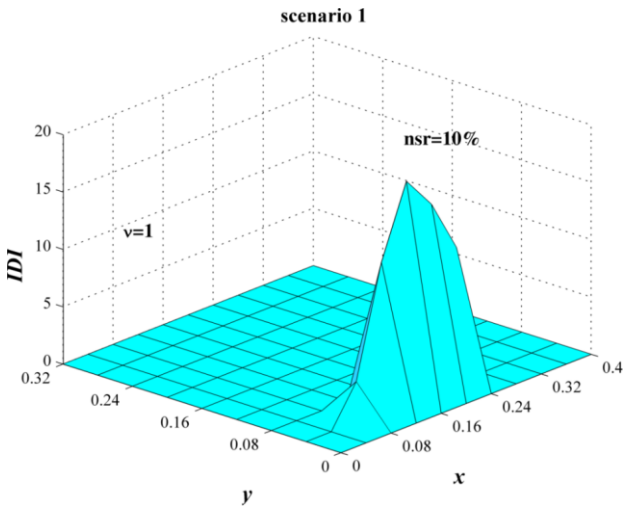

Figure 20. Results for scenario 1. *nsr* 10%, P_f =15%

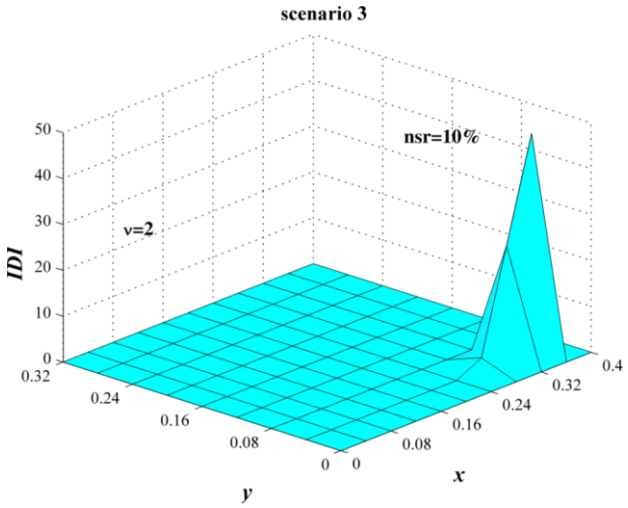

Figure 21. Results for scenario 3. *nsr* =10%, P_f =3%

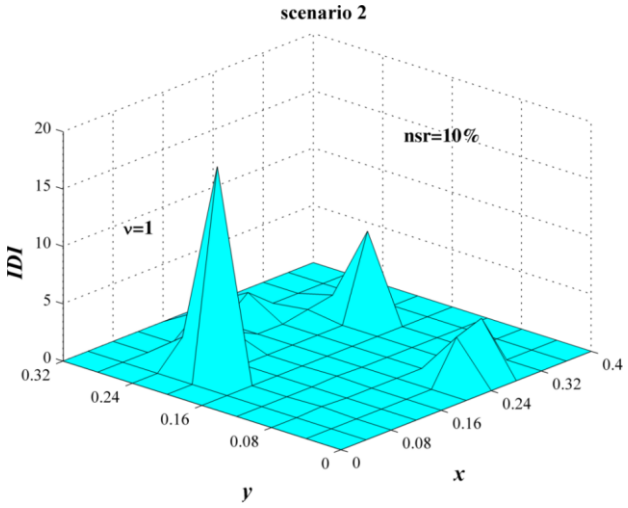

Figure 22. Results for scenario 2. *nsr* =10%, P_f =15%

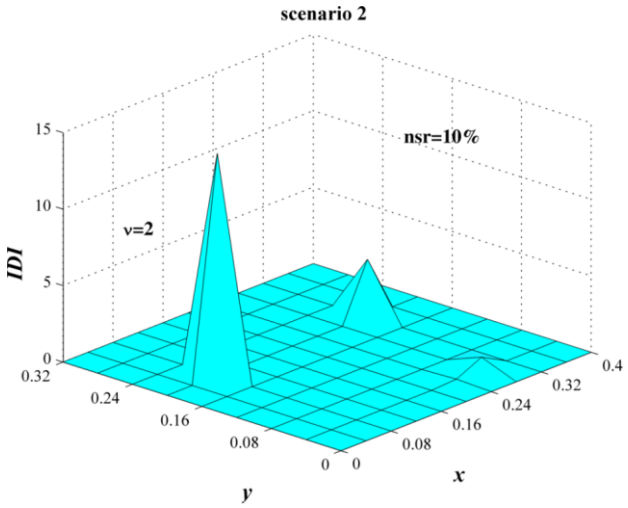

Figure 23. Results for scenario 2. *nsr* =10%, P_f =3%

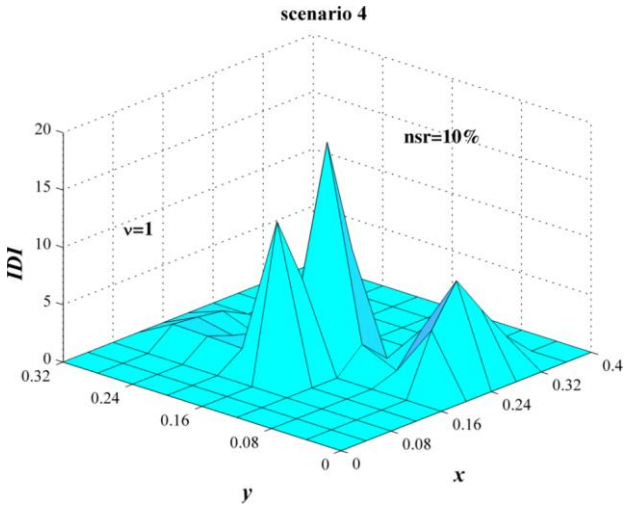

Figure 24. Results for scenario 4. *nsr* =10%, P_f =15%

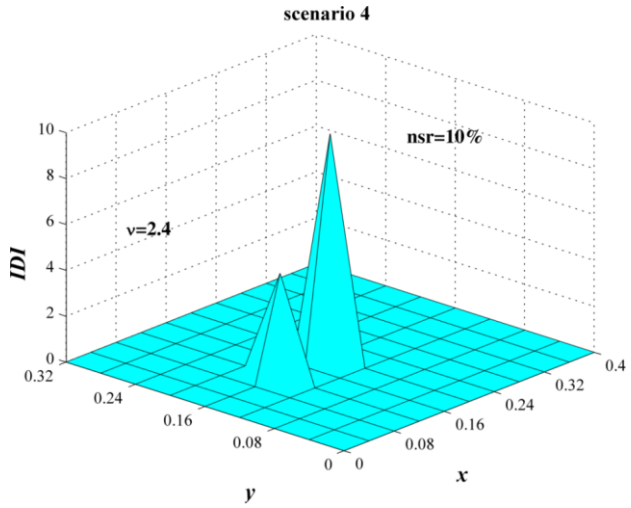

Figure 25. Results for scenario 2. *nsr* =10%, P_f =1%

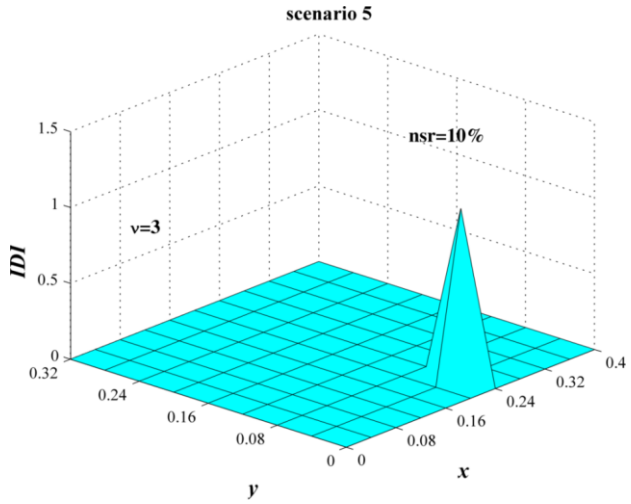

Figure 26. Results for scenario 5. Reduction of stiffness of 15%. P_f =0.3%

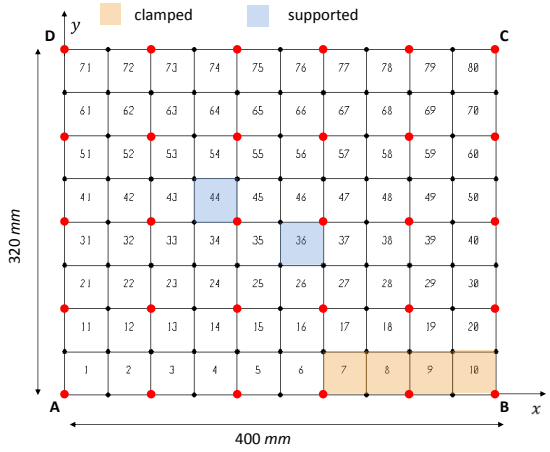

Figure 27. Grid of 30 sensors (red dots)

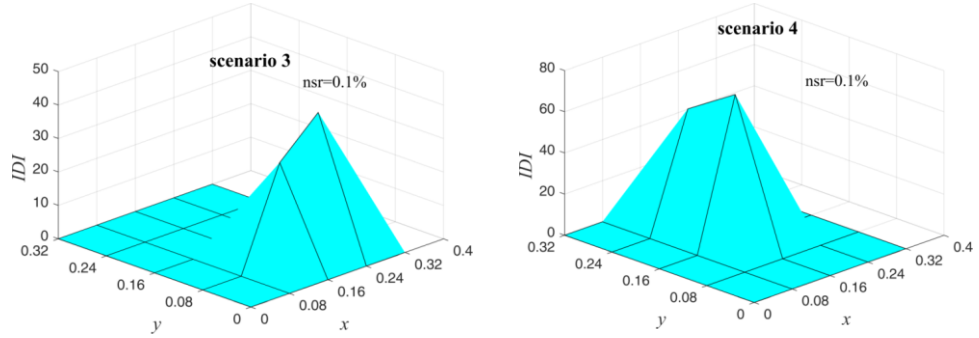

Figure 2827. Results for scenario 3(left) and 4 (right) using the grid of 30 sensors in Figure 27~~Figure 27~~

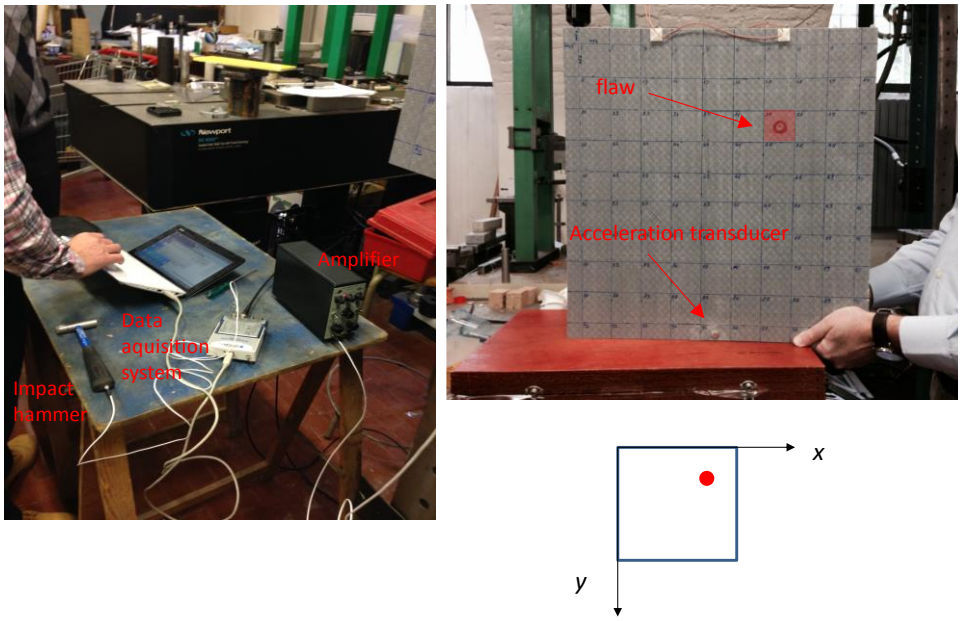

Figure 2927. Composite plate and flaw induced.

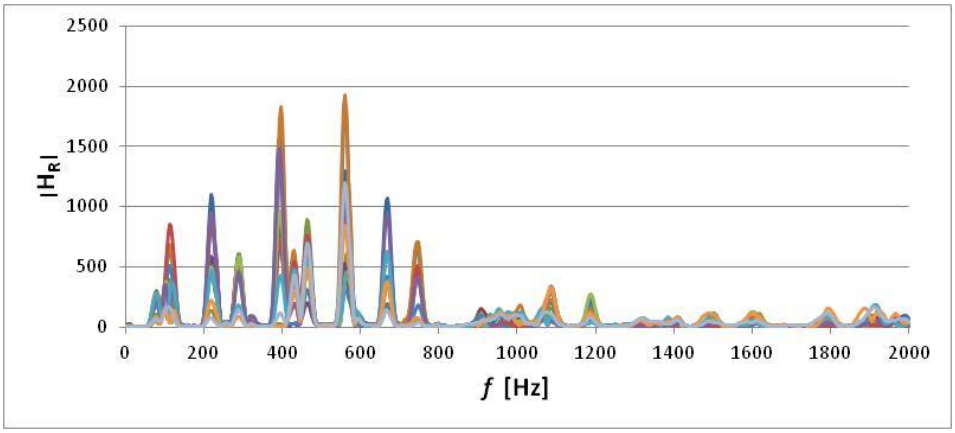

Figure 3028. Composite plate. Magnitude of FRFs at the nodes of the plate

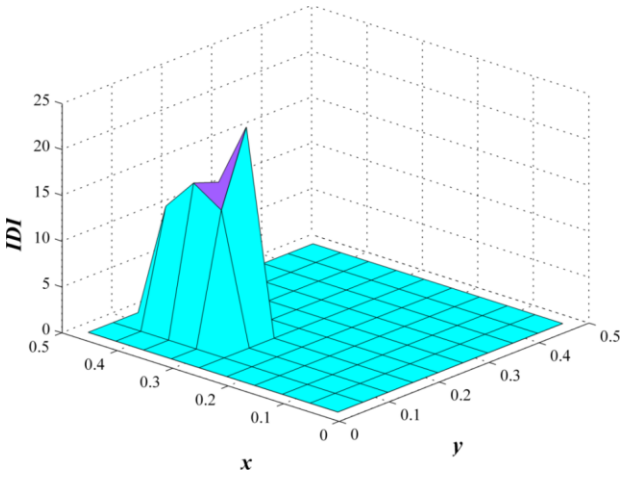

Figure 31~~29~~. Results for the damage induced in the composite plate

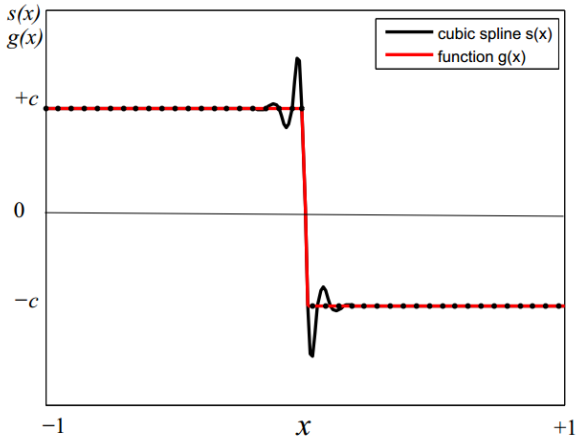

Figure 32~~30~~. Gibbs phenomenon for cubic splines

Table 1

Damage scenarios

Scenario		*Element n.*	*Damage*
1	Clamped plate	3 and 7	15%
		4 and 6	25%
		5	50%
2	Supported plate	28	15%
		58	25%
		53	50%
3	Clamped plate	7	25%
		8 and 9	50%
		10	75%
4	Supported plate	36 and 44	50%
5	Clamped plate	7	15%